

Charge density wave and pressure-dependent superconductivity in the kagome metal CsV_3Sb_5 : A first-principles study

Jian-Guo Si,^{1,2} Wen-Jian Lu,^{3,*} Yu-Ping Sun,^{3,4,5} Peng-Fei Liu^{①,1,2} and Bao-Tian Wang^{①,2,6,†}

¹*Institute of High Energy Physics, Chinese Academy of Sciences, Beijing 100049, China*

²*Spallation Neutron Source Science Center, Dongguan 523803, China*

³*Key Laboratory of Materials Physics, Institute of Solid State Physics, Chinese Academy of Sciences, Hefei 230031, China*

⁴*High Magnetic Field Laboratory, Chinese Academy of Sciences, Hefei 230031, China*

⁵*Collaborative Innovation Center of Microstructures, Nanjing University, Nanjing 210093, China*

⁶*Collaborative Innovation Center of Extreme Optics, Shanxi University, Taiyuan, Shanxi 030006, China*



(Received 29 November 2021; accepted 11 January 2022; published 21 January 2022)

The kagome metals $AV_3\text{Sb}_5$ ($A = \text{K}, \text{Rb}, \text{and Cs}$) have received intensive research interest due to the presence of charge density waves (CDWs), \mathbb{Z}_2 topological surface states, and intriguing pressure-dependent superconductivity. Using first-principles calculations, here we study the origin of the CDW order in CsV_3Sb_5 and its superconducting properties under pressure up to 45 GPa. We reveal that the momentum-dependent electron-phonon coupling (EPC) effect plays an important role in the formation of the CDW order. Upon compression, the movement of the van Hove singularity, which induces the change in the density of states at the Fermi level, as well as the redistribution of the EPC, can explain the experimentally observed double superconducting domes. The main contribution to the EPC is varied from in-plane vibrational modes in superconducting area I (2–15 GPa) to out-of-plane modes in superconducting area II (15–45 GPa). Our observations clarify the origin of the CDW order and shed some light on understanding the experimental observations of pressure-dependent superconductivity in CsV_3Sb_5 .

DOI: [10.1103/PhysRevB.105.024517](https://doi.org/10.1103/PhysRevB.105.024517)

I. INTRODUCTION

The kagome lattice, composed of two corner-sharing triangles, has attracted considerable attention due to its inherent geometrical frustration inducing many intriguing phenomena, such as chiral physics [1–3], spin liquid states [4,5], magnetic topological states [6,7], the anomalous Hall effect (AHE) [8–10], superconducting states [11,12], etc. Recently, Ortiz *et al.* discovered a new family of kagome metals, $AV_3\text{Sb}_5$ ($A = \text{K}, \text{Rb}, \text{and Cs}$), which exhibit a structurally perfect kagome net of vanadium [13]. The transport properties and scanning tunneling microscopy (STM) measurements revealed that the $AV_3\text{Sb}_5$ family materials undergo a charge density wave (CDW) transition with transition temperatures of $T_{\text{CDW}} = 80, 102, \text{ and } 94$ K for $A = \text{K}, \text{Rb}, \text{ and Cs}$ [14–19], respectively. When the temperature decreases to 2.5, 0.93, and 0.92 K, CsV_3Sb_5 , KV_3Sb_5 , and RbV_3Sb_5 , respectively, enter a superconducting ground state [12,14–16,19,20]. Band structure calculations showed that $AV_3\text{Sb}_5$ metals have multiple topologically nontrivial band crossings in close proximity to the Fermi level [12,13,20], consistent with angle-resolved photoemission spectroscopy (ARPES) measurements and observations of Shubnikov–de Haas oscillations [12,14,15]. In addition, the concurrence of the AHE was also reported in CsV_3Sb_5 and KV_3Sb_5 [17,21]. Such rich quantum phenomena

make the $AV_3\text{Sb}_5$ family the star materials to investigate the relationship among CDW order, superconductivity, and non-trivial electronic states, sparking intense research interest.

High pressure can effectively manipulate the crystal structures and further tune the corresponding band structures and properties without introducing impurities. It has been widely used to induce superconductivity and study the relationship between superconductivity and other phenomena, such as CDWs in TaS_2 [22,23] and magnetoresistance in MoTe_2 and WTe_2 [24,25]. For the $AV_3\text{Sb}_5$ family materials, the superconductivity shows unique pressure-dependent characters. Recently, two research groups studied the evolution of CDWs and superconductivity in CsV_3Sb_5 under high pressure via electrical transport and magnetic susceptibility measurements [26,27]. They reported a double-peak superconducting phase diagram before reaching the pressure of 9 GPa. The maximum superconducting transition temperature T_c of 8 K was observed at ~ 2 GPa, when the CDW is completely suppressed. Such pressure-induced double-peak superconducting behavior was also found in its isostructural compounds KV_3Sb_5 and RbV_3Sb_5 [28–30]. By further increasing the pressure, Zhang *et al.* observed the gradual decrease and disappearance of the superconductivity from 0.8 to 7.5 GPa in CsV_3Sb_5 [31]. Then, they reported the reemergence of the superconductivity in CsV_3Sb_5 at around 16.5 GPa, which keeps robust up to 47.9 GPa and was attributed to a pressure-induced Lifshitz transition [31]. Some other groups also studied the pressure-controlled CDW order and the superconductivity in CsV_3Sb_5 up to 50 GPa [19,32,33]. The CDW order is

*Corresponding author: wjlu@issp.ac.cn

†Corresponding author: wangbt@ihep.ac.cn

monotonically suppressed, and the superconductivity exhibits a pressure-dependent double-dome phase diagram. However, the details of the electronic structure and electron-phonon coupling (EPC) properties of the kagome lattice CsV_3Sb_5 are scarce from a theoretical point of view.

In this paper, we have systematically investigated the electronic properties and the EPC of the kagome metal CsV_3Sb_5 via first-principles calculations. Our calculated results of phonon dispersion and phonon linewidth show that the momentum-dependent EPC plays a significant role in the formation of the CDW order. The electronic density of states (DOS) at the Fermi level $[N(E_F)]$ is changed by external pressure. The van Hove singularity as well as the EPC is greatly modulated. According to our results, the pressure-dependent evolution of the superconductivity is still within the framework of the Bardeen-Cooper-Schrieffer (BCS) theory. The vibration mode analysis shows that the main contribution to the superconductivity is varied from in-plane phonon modes to the out-of-plane phonon modes with increasing pressure. The soft phonon mode, which is in tight relation with the EPC, gradually disappears in the $q_z = 0.5$ plane and reappears in the $q_z = 0$ plane. In addition, the nontrivial \mathbb{Z}_2 nature remains robust under pressure up to 45 GPa. Our observations clarify the origin of the formation of CDW order and are conducive to understanding the experimental observations of the pressure-dependent superconductivity in CsV_3Sb_5 .

II. COMPUTATIONAL DETAILS

The first-principles calculations were performed based on density functional theory (DFT) as implemented in the QUANTUM ESPRESSO package [34]. The interaction between the electrons and ionic cores was treated by the ultrasoft pseudopotentials [35]. The exchange-correlation interaction was described by the generalized gradient approximation (GGA) and parameterized by the Perdew-Burke-Ernzerhof functional [36]. In order to conduct the van der Waals correction accurately, the zero-damping DFT-D3 functional was employed in all the calculations [37]. The cutoff energies of the wave functions and charge density were set as 60 and 600 Ry, respectively. The Gaussian smearing method was used to calculate the charge density with a smearing parameter of $\sigma = 0.01$ Ry. All structures were fully relaxed until the Hellmann-Feynman force acting on each atom was less than 10^{-5} Ry/Å, and the convergence criterion for self-consistent calculations was set to be 10^{-6} Ry. The Brillouin zone (BZ) was sampled on a $10 \times 10 \times 6$ mesh of k points. Phonon dispersion curves of the normal state were calculated based on density functional perturbation theory [38], where a denser $20 \times 20 \times 12$ k -point grid and a $5 \times 5 \times 3$ q -point grid were employed for the EPC calculations. The phonon-related calculations were carried out without including the spin-orbit coupling (SOC) effect, because it is less important in describing the vibrational properties [39–41]. The surface states were calculated by the iterative Green's function as provided in the WANNIERTOOLS package [42,43], where a tight-binding method based on the maximally localized Wannier function (MLWF) was employed [44,45].

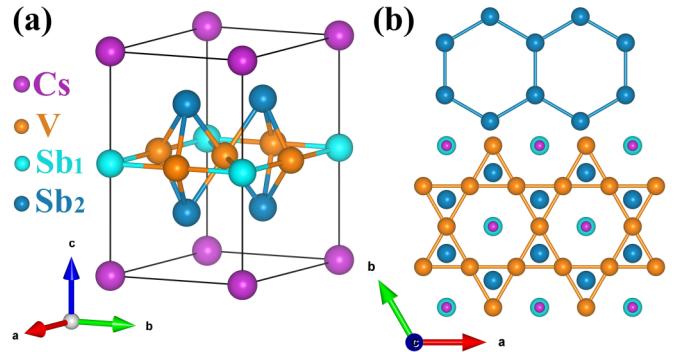


FIG. 1. (a) Crystal structure of CsV_3Sb_5 . The Cs, V, and Sb₁ (Sb₂) atoms are presented as purple, orange, and azure (steel blue) balls, respectively. (b) The graphite net formed by Sb₂ atoms (top) and the two-dimensional kagome lattice formed by V atoms (bottom).

III. RESULTS AND DISCUSSION

A. Crystal and electronic structures at zero pressure

The V-based kagome metal CsV_3Sb_5 was previously synthesized by the self-flux method and was characterized by x-ray diffraction [12,14]. It crystallizes in a hexagonal space group of $P6/mmm$ (No. 191). As shown in Fig. 1(a), the crystal is formed by V_3Sb_5 slabs stacking along the c axis through van der Waals interactions, while the Cs atoms insert themselves into the adjacent slabs. The V atoms form a perfect kagome lattice in the V-Sb slab. The Sb atoms occupy two unequal atomic positions: Sb₁ and Sb₂. The Sb₁ atoms locate at the centers of the hexagons in the V-Sb slabs, while the Sb₂ atoms form a graphite net, as displayed in Fig. 1(b). Due to the layered nature of the CsV_3Sb_5 structure, we use DFT-D3 to obtain accurate structural parameters; DFT-D3 has been proven to be an effective method for the structure optimization of the kagome metals AV_3Sb_5 [46–49]. The fully relaxed lattice constants a and c are 5.454 and 9.330 Å, respectively, which are comparable to previous experimental and theoretical results [12,13,50]. The calculated orbital-resolved band structure of normal-state CsV_3Sb_5 is shown in Fig. 2(a). Without including the SOC, there are two bands crossing the Fermi level. The two bands crossing the Fermi level around the Γ and A points are mainly contributed by the out-of-plane orbitals of Sb p_z (orange balls), and the bands around the M and L points

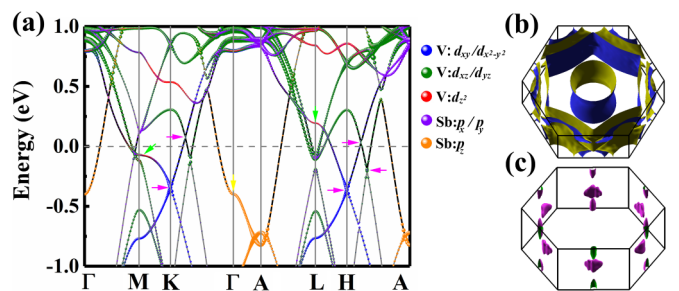


FIG. 2. (a) Orbital-resolved band structure without SOC and (b) and (c) Fermi surfaces of the pristine phase of CsV_3Sb_5 . In (a), the van Hove singularities are marked with green and yellow arrows, and the multiple Dirac points are marked with magenta arrows.

are dominated by the out-of-plane orbitals of V d_{xz}/d_{yz} (green balls). These results are consistent with the previous DFT results [14,27]. Figures 2(b) and 2(c) show the corresponding Fermi surfaces, which show quasi-two-dimensional and highly anisotropic characters. Such highly two-dimensional character favors the formation of the CDW order through the nesting scattering [18]. For the kagome lattice CsV_3Sb_5 , there are three van Hove singularities (or saddle points) located at Γ (-398 meV), M (-74 meV), and L (193 meV) points, as shown in Fig. 2(a). While the former one (the yellow arrow) is mainly composed of the Sb p_z orbitals, the latter two (the green arrows) are mainly contributed from the out-of-plane orbitals of V d_{z^2} . Using the optical spectroscopy method, Zhou *et al.* attested that the van Hove singularity nesting is very important in driving the CDW instability in CsV_3Sb_5 [51]. We also find multiple Dirac points, which are dominated by the in-plane orbitals of V $d_{xy}/d_{x^2-y^2}$, in proximity to the Fermi level (the purple arrows), agreeing well with one previous DFT report [52].

After including SOC, as shown in Supplemental Fig. S1(a) [53], a symmetry-enforced continuous direct gap near the Fermi level as marked by the color shade creates a nontrivial topological invariant. In Supplemental Figs. S1(b) and S1(c) and Supplemental Table SI [53], we show the calculated surface states and parity of the bands at the time-reversal invariant momentum (TRIM) points, respectively. Both of them identify the kagome structure of CsV_3Sb_5 as a \mathbb{Z}_2 topological metal [12].

B. Origin of CDW order under ambient pressure

The magnetization, electrical resistivity, and heat capacity of the kagome metal CsV_3Sb_5 exhibit a clear anomaly at 94 K [12], suspected to be an electronic instability. It was subsequently confirmed as a $2 \times 2 \times 2$ CDW transition by STM, hard x-ray scattering, and ARPES measurements [18,54,55]. The mainstream views on the origin of the CDW formation in two-dimensional materials are Fermi-surface nesting [56,57], momentum-dependent EPC [58–60], and exciton condensation (electron-hole coupling) [61,62]. The CDW formation in the kagome metal CsV_3Sb_5 was previously understood as the electronic instability [46], saddle-point nesting [51], and Jahn-Teller-like instability [63], etc.

The Fermi-surface nesting is always evaluated by calculating the electron susceptibility [59,64]. Using the calculated Fermi surface in Figs. 2(b) and 2(c), we calculate the electron susceptibility as plotted in Supplemental Fig. S2 [53]. We find that both positions of the maximal real and imaginary parts (around $\frac{1}{2} \Gamma M$) of the electron susceptibility deviate from the Q_{CDW} . This fact clearly indicates that the Fermi-surface nesting effect cannot account for the formation of the CDW order in CsV_3Sb_5 . Besides, the exciton condensation especially works for some semimetals, such as TiSe_2 [61,62]. Thus here we evaluate the momentum-dependent EPC effect on the formation of the CDW order in CsV_3Sb_5 . Our calculated phonon dispersions of the normal-state CsV_3Sb_5 under ambient pressure are shown in Fig. 3(a). We find two remarkably imaginary phonon points locating at the high-symmetry points of M and L , consistent with one previous report [46]. Both of those points have the same in-plane projection ($\frac{1}{2}a^*$), which

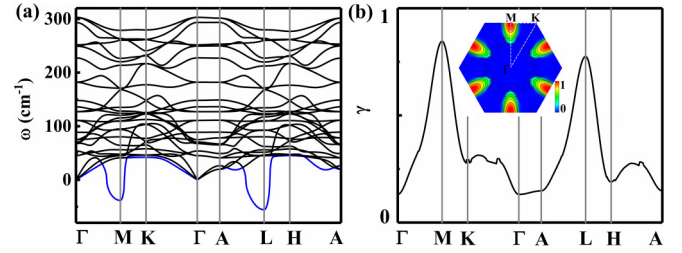


FIG. 3. (a) Phonon dispersions and (b) total phonon linewidth of CsV_3Sb_5 under ambient pressure. The inset of (b) is the phonon linewidth γ of the lowest mode in the BZ.

equals to the vector of the CDW order, standing for the in-plane part of the $2 \times 2 \times 2$ CDW superstructure in real space. We also evaluate the phonon linewidth γ , which is directly related to the strength of the EPC. The γ is defined as

$$\gamma_{qv} = 2\pi\omega_{qv} \sum_{ij} \int \frac{d^3k}{\Omega_{\text{BZ}}} |g_{qv}(k, i, j)|^2 \times \delta(\varepsilon_{q,i} - \varepsilon_F) \delta(\varepsilon_{k+q,j} - \varepsilon_F), \quad (1)$$

where the $g_{qv}(k, i, j)$ is the EPC matrix and can be calculated by

$$g_{qv}(k, i, j) = \left(\frac{\hbar}{2M\omega_{qv}} \right)^{1/2} \left\langle \psi_{i,k} \left| \frac{dV_{\text{SCF}}}{d\hat{u}_{qv}} \hat{\xi}_{qv} \right| \psi_{j,k+q} \right\rangle. \quad (2)$$

Here, ψ is the wave function, V_{SCF} is the Kohn-Sham potential, \hat{u} is atomic displacement, and $\hat{\xi}$ is the phonon eigenvector. The calculated normalized total phonon linewidth along the high-symmetry path is shown in Fig. 3(b). We can see that there are two peaks at the high-symmetry points of M and L . The inset of Fig. 3(b) shows the phonon linewidth of the lowest mode in the plane of $q_z = 0$. The areas with the highest value (the red areas) also locate at the M point (the vector of the CDW), according well with the results of phonon dispersions. Therefore we conclude that the momentum-dependent EPC effect is important for the formation of the CDW order in CsV_3Sb_5 .

C. Superconductivity under high pressure

An old but longstanding issue is the relationship between CDW order and superconductivity. The competition [22,23,65,66] or coexistence [67,68] between CDW order and superconductivity in transition metal dichalcogenides (TMDs) has greatly attracted research interest. For the kagome metal CsV_3Sb_5 , the pressure-induced behaviors of the CDW order and superconductivity were also widely studied in experiments [19,26,27,29,32,33]. Both the CDW order and superconductivity were detected within 2 GPa, but it is difficult to quantitatively obtain the ratio of the CDW superstructure and the high-symmetry phase by both experiment detections and theoretical calculations. Therefore we focus on the dependence of the superconducting transition in the kagome metal CsV_3Sb_5 on pressure when the CDW order is fully suppressed under 2 GPa. We want to explain why there exist double domes in its pressure-dependent superconducting phase diagram.

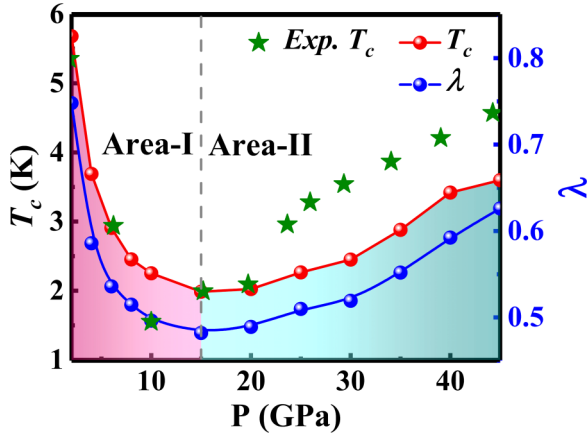


FIG. 4. The evolutions of T_c (red line) and EPC constant λ (blue line) of CsV_3Sb_5 as functions of pressure. The experimental values of T_c are from Ref. [33].

The superconducting transition temperature T_c is estimated by the Allen-Dynes-modified McMillan formula [69,70]:

$$T_c = \frac{\omega_{\log}}{1.2} \exp\left(-\frac{1.04(1+\lambda)}{\lambda - \mu^* - 0.62\lambda\mu^*}\right). \quad (3)$$

The μ^* is the Coulomb pseudopotential and can be generally set as a typical value of 0.1 [71,72]. The logarithmically averaged phonon frequency ω_{\log} is defined as

$$\omega_{\log} = \exp\left(\frac{2}{\lambda} \int \frac{d\omega}{\omega} \alpha^2 F(\omega) \log \omega\right), \quad (4)$$

where $\alpha^2 F(\omega)$ is the Eliashberg spectral function and can be calculated by

$$\alpha^2 F(\omega) = \frac{1}{2\pi N(E_F)} \sum_{q\nu} \delta(\omega - \omega_{q\nu}) \frac{\gamma_{q\nu}}{\hbar\omega_{q\nu}}. \quad (5)$$

Here, $\gamma_{q\nu}$ is the phonon linewidth, which can be calculated by Eq. (2). The total EPC constant λ can be computed as follows:

$$\lambda = \sum_{q\nu} \lambda_{q\nu} = 2 \int \frac{\alpha^2 F(\omega)}{\omega} d\omega. \quad (6)$$

Figure 4 shows the calculated pressure-dependent phase diagram of the T_c for CsV_3Sb_5 . The experimental results from Ref. [33] are also plotted for comparison. We can see that the evolution of our calculated T_c is consistent with the experimental data [19,32,33]. The T_c decreases from 5.68 K (2 GPa) to the minimum of 1.97 K (15 GPa) firstly and then increases to 3.6 K under a pressure of 45 GPa. Based on the BCS theory, the superconductivity is strongly dependent on the EPC. We calculate the EPC under different pressures and present them in Fig. 4. One can see that the T_c and the EPC have almost the same pressure-dependent trends. The λ decreases from 0.71 (2 GPa) to 0.48 (15 GPa) firstly and then increases to 0.63 at 45 GPa. Therefore we can conclude that the superconductivity of CsV_3Sb_5 under pressure, in the double domes, still belongs to a conventional BCS weak superconductor. It is worth noting that a previous study also evaluated the strength of the EPC [46]; its calculated results show that the λ is only 0.25 for the

CsV_3Sb_5 with an inverse Star of David (ISD) superstructure. Such a difference is mainly due to the λ in this paper being approximated by only considering the breathing mode.

In order to shed light on the phase diagram of the superconducting temperature, in the following, we selected three special pressure points (2, 15, and 45 GPa) to analyze the phonon dispersions and electronic structures in detail.

The phonon dispersions of CsV_3Sb_5 under 2, 15, and 45 GPa are shown in Figs. 5(a)–5(c), respectively. We can see that the phonon frequencies are obviously increased with increasing pressure. Such pressure-induced increases in the phonon vibrations in E space (frequency space) are common and have been observed in many systems [73,74]. Compared with the phonon dispersion curves of the normal-state CsV_3Sb_5 under ambient pressure [see Fig. 3(a)], the imaginary frequencies under 2 GPa are missing, indicating the full suppression of its CDW order. This is consistent with recent experimental observations [26,27]. For the phonon spectrum of CsV_3Sb_5 under 2 GPa, one can see that there are several soft modes around the L point. Such modes will contribute evidently to the EPC, according to Eq. (6). With increasing pressure, the soft modes in the plane of $q_z = 0.5$ (along the A - L - H - A direction) gradually disappear, and the lowest mode gradually creates a new soft mode at the M point, in the plane of $q_z = 0$. Further increasing the pressure to 50 GPa, the imaginary frequencies appear at the M point (see Supplemental Fig. S3 [53]). This indicates that the system is dynamically unstable at such high pressure and will form some new structures, such as the reemergence of a CDW order. It should be noted that a very recent theoretical study also predicted a possible CDW order under 35 GPa [75]. The difference between their and our predicted critical pressures (35 and 50 GPa) can be attributed to the difference in the computational parameters. Further experimental work is definitely needed to clarify this.

Figures 5(d)–5(f) show the atomic-vibrational-mode-resolved phonon spectra and the phonon density of states (PhDOS). One can see that the soft mode at the plane of $q_z = 0.5$ under 2 GPa is dominated by the in-plane modes of V xy and it is gradually suppressed by pressure. Under 45 GPa, the out-of-plane vibration mode of Cs z has an obvious contribution to the lowest soft phonon mode around the M point. In addition, our calculated PhDOS shows that the localized Cs atomic vibrations in the E space are greatly broadened by increasing pressure. The Sb atomic vibrations occupy a wide frequency range, which is evidently increased from 10–180 cm^{-1} at 2 GPa to 10–250 cm^{-1} at 45 GPa. The V atoms are relatively light, and their vibrations are mainly in the high-frequency range, which is also increased from 180–300 cm^{-1} at 2 GPa to 250–410 cm^{-1} at 45 GPa.

The EPC integrated over all phonon branches and distributed in the $q_z = 0$ and 0.5 planes of the BZ is drawn in Fig. 6. Upon compression, the redistribution of the EPC in the BZ is evident. Under 2 GPa, the areas with large EPC locate around the M and L points, which are mainly contributed by M-II and M-I, respectively [see Fig. 5(a)]. The EPC at the L points is larger than that at the M points. The large EPC areas under 2 GPa are localized at the boundary of the BZ. Increasing the pressure to 15 GPa, the distribution of the EPC becomes more homogeneous but still localizes at the

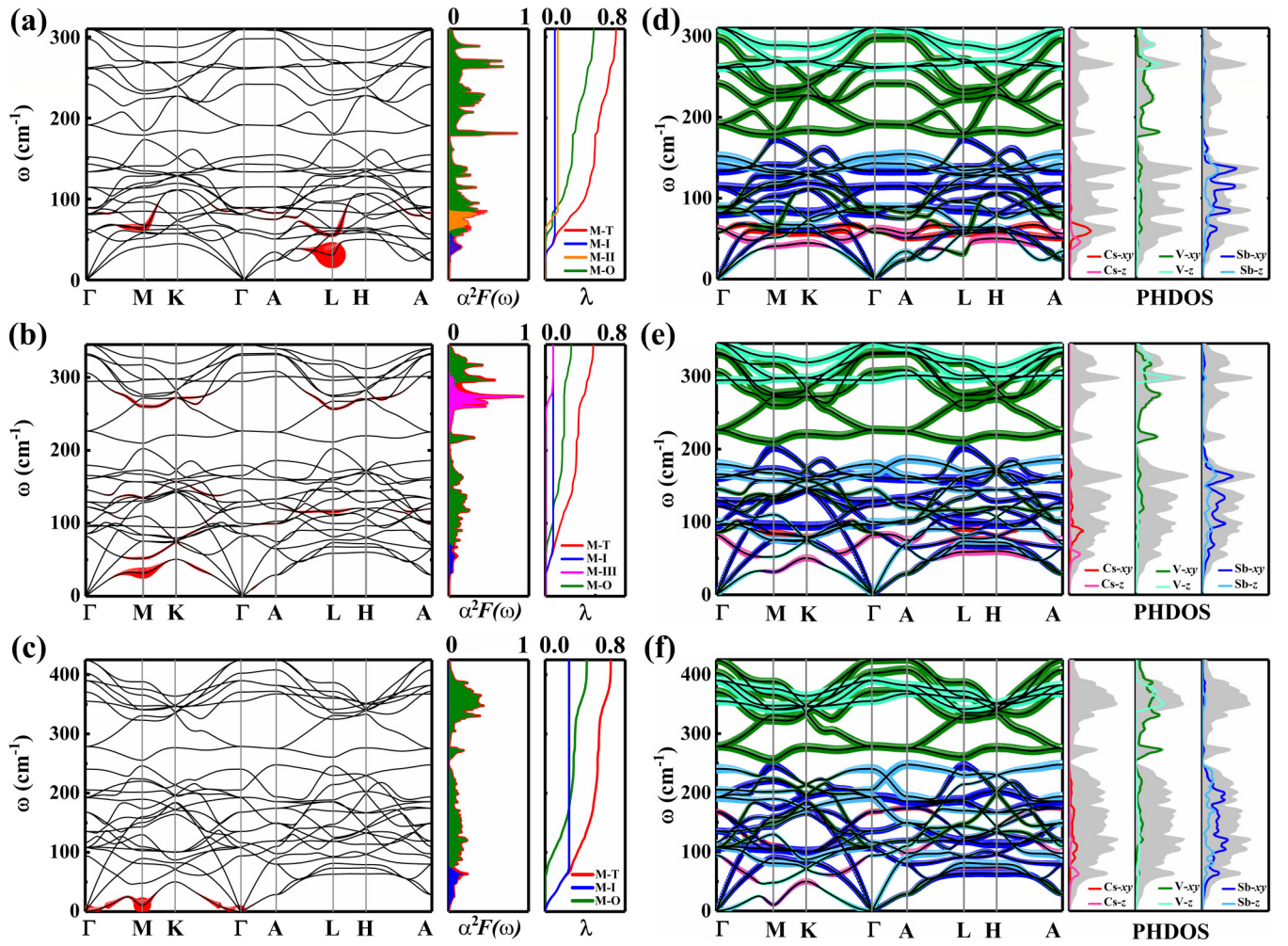


FIG. 5. Phonon dispersions weighted by the magnitude of the EPC, the mode-resolved Eliashberg spectral function $\alpha^2 F(\omega)$, and the integrated strength of EPC (λ) of CsV_3Sb_5 under (a) 2, (b) 15, and (c) 45 GPa. In order to visualize this clearly, the EPC is only plotted above 10 cm^{-1} , and the EPC of the lowest mode is plotted with a scale factor (0.4) for 45 GPa. M-T represents total phonon modes. M-I indicates the two lowest modes. M-II in (a) and M-III in (b) indicate modes 5 and 6 under 2 GPa and modes 20 to 22 under 15 GPa, respectively. M-O represents the other modes without the front special instructions. Phonon dispersions weighted by the vibrational modes of different atoms and the PhDOS for CsV_3Sb_5 under (d) 2, (e) 15, and (f) 45 GPa. The gray-shaded zone indicates the total PhDOS.

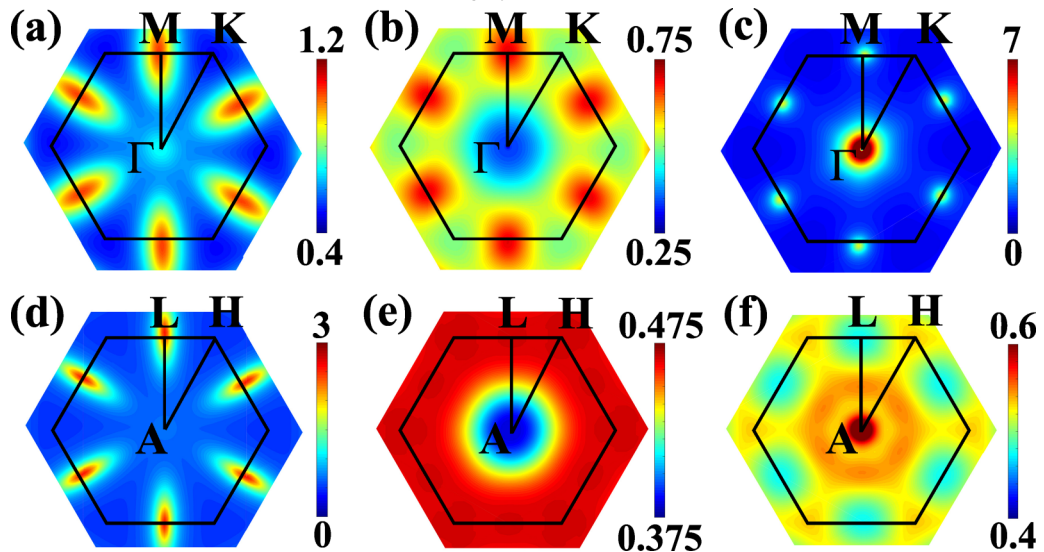


FIG. 6. The integrated EPC distributions of CsV_3Sb_5 in the plane of $q_z = 0$ under (a) 2, (b) 15, and (c) 45 GPa. The results for the plane of $q_z = 0.5$ are plotted in (d)–(f), respectively.

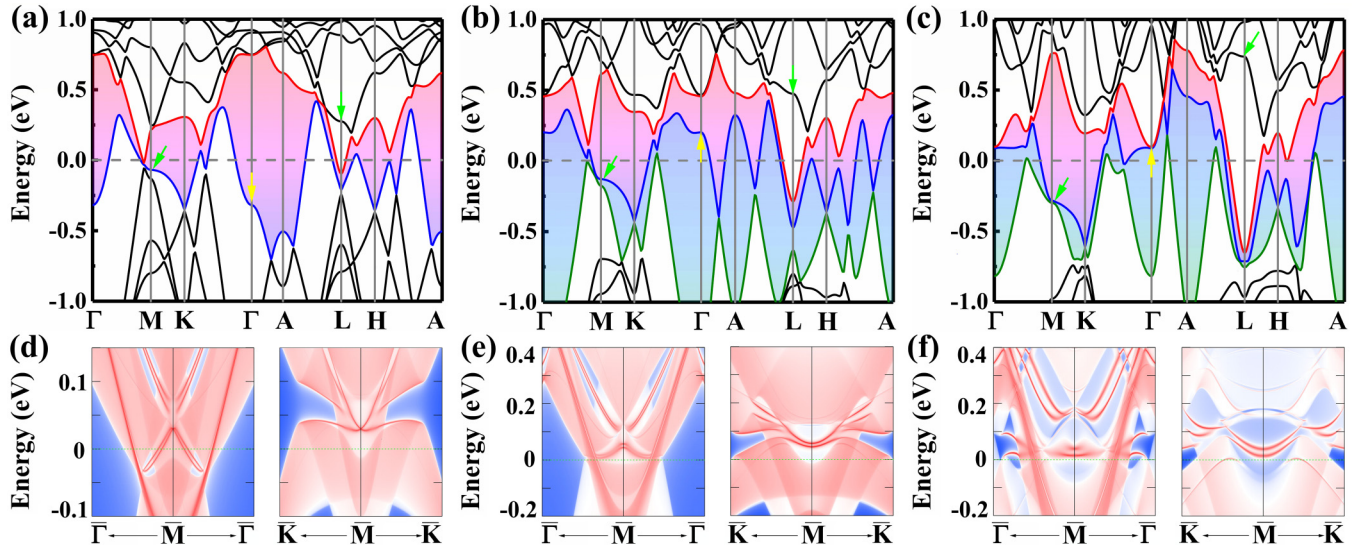


FIG. 7. Band structures with SOC of CsV_3Sb_5 under (a) 2, (b) 15, and (c) 45 GPa. For simplicity, the blue, red, and green lines can be indexed as band I, band II, and band III, respectively. Here, band I is the highest occupied band. The van Hove singularities are marked by arrows. Their corresponding surface states are plotted in (d)–(f).

boundary as well as at the M points. The plane with a large value of EPC is changed from $q_z = 0.5$ at 2 GPa to $q_z = 0$ at 15 GPa, which is consistent with the change in the soft phonon modes mentioned above. Further compressing to 45 GPa, the large EPC areas are localized near the Γ and A points. The EPC values around the Γ point are obviously larger than those around the A points. The M points still have localized large EPC. The relatively larger EPC plane is in $q_z = 0$. Overall, the main distribution of the EPC changes from the $q_z = 0.5$ plane to the $q_z = 0$ plane and undergoes transitions of localization-delocalization-relocalization.

To distinguish the modes' contribution to the superconductivity, we compare the phonon dispersions weighted by the magnitude of EPC in Figs. 5(a)–5(c) and weighted by vibration modes of different atoms in Figs. 5(d)–5(f). We can see that the EPC under 2 GPa is mainly contributed by the V - xy vibrations, especially for M-I and M-II. Compressing to 15 GPa, the EPC is mainly derived from the in-plane mode of V - xy -dominated M-III and the out-of-plane-vibration-dominated M-I along Γ - M - K - Γ . Further increasing pressure to 45 GPa, the high-frequency modes have less contribution to the superconductivity, while the contribution of the lowest two phonon modes (M-I) to the EPC reaches to 36.5%. The M-I are dominated by the out-of-plane vibration modes. In short, we can conclude that the main contribution to the EPC and superconductivity is changed from in-plane vibration modes to the out-of-plane vibration modes with increasing pressure from 2 to 45 GPa.

The calculated band structures of CsV_3Sb_5 under 2, 15, and 45 GPa are shown in Figs. 7(a)–7(c). Compared with the band structure under 2 GPa, we can see that there is one more band crossing the Fermi level [the olive band in Fig. 7(b)]. This clearly indicates that the system has undergone a Lifshitz transition. Zhang *et al.* observed such a pressure-induced Lifshitz transition by evaluating the c -to- a ratio, and they proposed that the reemergence of the superconductivity can be attributed to the Fermi-surface reconstruction caused by such

a transition [31]. Here, we can define the two-band superconductivity area, area I, and three-band superconductivity area, area II, according to the critical pressure point of the Lifshitz transition, as shown in Fig. 4. This definition is similar to the experimentally reported superconducting (SC) areas SC-I and SC-II or double domes in Refs. [19,32,33]. The multiband superconductivity in the kagome metal CsV_3Sb_5 was also confirmed by scanning tunneling spectroscopy [76].

Comparing the band structure under 15 GPa with respect to that under 2 GPa, the bandwidth of the original two bands that crossed the Fermi level [shown by red and blue lines in Fig. 7(b)] is evidently reduced. Such kind of pressure effect has also been observed in $1T$ - TiTe_2 [74], where uniaxial pressure was found to be able to increase the $N(E_F)$ and T_c . However, in our case, the $N(E_F)$ decreases from 5.5 states/eV under 2 GPa to 3.89 states/eV under 15 GPa. This decreasing trend of the $N(E_F)$ is also consistent with the decrease in T_c in area I (see Fig. 4). In addition, the van Hove singularities located at the M and L points [the green arrows in Figs. 7(a)–7(c)] move gradually away from the Fermi level. This may induce the decrease in $N(E_F)$. As indicated by the yellow arrows in Figs. 7(a) and 7(b), the van Hove singularity at the Γ point moves from -321 to 200 meV by increasing pressure from 2 to 15 GPa, which is mainly contributed by the $\text{Sb} - p_z$ orbitals (see Supplemental Fig. S4(b) [53]). Further compressing to 45 GPa, the dispersion of the original two bands (shown by red and blue lines) becomes strong again, while the olive one is reduced significantly [see Fig. 7(c)]. The V - d_{z^2} -dominated van Hove singularity located at the Γ point is pressure induced close to the Fermi level, accompanied with an increase in the $N(E_F)$ [the calculated $N(E_F)$ is 4.32 states/eV at 45 GPa]. This can explain to some extent the pressure-induced enhancement of the superconductivity in area II. In fact, the van Hove singularity is very important for the superconductivity, such as the chiral superconductivity arising in graphene when the van Hove singularity moves to the Fermi level by doping [77–79], and strong coupling between the van Hove singularity and

phonon in PdTe₂ [80]. The pressure-induced movements of the van Hove singularities in CsV₃Sb₅ may be a key factor for the modulation of $N(E_F)$ as well as T_c . Combining these results with our EPC results, we can understand the pressure-dependent phase diagram of the T_c and can conclude that the superconductivity of CsV₃Sb₅ under different pressures (at least in the experimentally observed double superconducting domes) is still following the framework of the BCS theory.

D. Topological properties under high pressure

The normal phase of CsV₃Sb₅ under ambient pressure is a \mathbb{Z}_2 topological metal, which can be categorized by analyzing the parity of the wave function at the TRIM points and analyzing the surface states [46]. In this paper, we extend such study to high pressure. Our calculated band structures with SOC of CsV₃Sb₅ under different pressures show that there are continuous band gaps across the whole BZ at the Fermi level, which are noted by the color shades in Figs. 7(a)–7(c). We also calculate the parity of the wave function of the bands crossing the Fermi level, as listed in Supplemental Table SI [53]. The results indicate that the kagome metal CsV₃Sb₅ keeps topologically nontrivial characters. The lowest unoccupied band (band II) is always nontrivial. The highest occupied band (band I) is nontrivial at 2 and 15 GPa. The surface states of CsV₃Sb₅ under 2, 15, and 45 GPa are shown in Figs. 7(d)–7(f). We can see that the calculated surface states under 2 GPa are very close to the previous results at zero pressure [46]. At 15 GPa, the crossed surface states at the \bar{M} point are split. Further increasing the pressure, the surface states become more complex. The maintenance of the nontrivial \mathbb{Z}_2 nature calls for experimental examination in the future.

IV. CONCLUSIONS

In conclusion, we have systematically investigated the origin of the CDW order and the high-pressure effects on the superconductivity in the kagome metal CsV₃Sb₅. Our results show that the momentum-dependent EPC plays an important role in the formation of the CDW order at ambient pressure. Under high pressure, the evolutions of the EPC and $N(E_F)$ are highly correlated with T_c in both superconducting area I and superconducting area II. The good agreement between our calculated T_c and the experimental results clearly supports the notion that the CsV₃Sb₅ is still a weak BCS superconductor, under pressure up to 45 GPa. The main contribution to the superconductivity is changed from the in-plane modes to the out-of-plane modes with increasing pressure. The main distribution of the EPC as well as the soft phonon modes is varied from the $q_z = 0.5$ plane in superconducting area I to the $q_z = 0$ plane in superconducting area II. The pressure-induced redistribution of the EPC as well as reemergence of the soft phonon modes may merit considering CsV₃Sb₅ to be a proper platform to investigate lattice instability and related phenomena. Our results may shed some light on understanding the experimental observations of the CDW order and the evolution of the superconductivity under high pressure in CsV₃Sb₅.

ACKNOWLEDGMENTS

The authors gratefully acknowledge financial support from the National Natural Science Foundation of China (Grants No. 11774351, No. 12104458, and No. 12074381). The authors also are thankful for the computational resources from the Hefei Advanced Computing Center and the Supercomputer Centre of the China Spallation Neutron Source.

-
- [1] S.-L. Yu and J.-X. Li, *Phys. Rev. B* **85**, 144402 (2012).
- [2] K. Ohgushi, S. Murakami, and N. Nagaosa, *Phys. Rev. B* **62**, R6065 (2000).
- [3] Z. Wang, Y.-X. Jiang, J.-X. Yin, Y. Li, G.-Y. Wang, H.-L. Huang, S. Shao, J. Liu, P. Zhu, N. Shumiya, M. S. Hossain, H. Liu, Y. Shi, J. Duan, X. Li, G. Chang, P. Dai, Z. Ye, G. Xu, Y. Wang *et al.*, *Phys. Rev. B* **104**, 075148 (2021).
- [4] S. Yan, D. A. Huse, and S. R. White, *Science* **332**, 1173 (2011).
- [5] T.-H. Han, J. S. Helton, S. Chu, D. G. Nocera, J. A. Rodriguez-Rivera, C. Broholm, and Y. S. Lee, *Nature (London)* **492**, 406 (2012).
- [6] D. F. Liu, A. J. Liang, E. K. Liu, Q. N. Xu, Y. W. Li, C. Chen, D. Pei, W. J. Shi, S. K. Mo, P. Dudin, T. Kim, C. Cacho, G. Li, Y. Sun, L. X. Yang, Z. K. Liu, S. S. P. Parkin, C. Felser, and Y. L. Chen, *Science* **365**, 1282 (2019).
- [7] L. Ye, M. Kang, J. Liu, F. von Cube, C. R. Wicker, T. Suzuki, C. Jozwiak, A. Bostwick, E. Rotenberg, D. C. Bell, L. Fu, R. Comin, and J. G. Checkelsky, *Nature (London)* **555**, 638 (2018).
- [8] E. Liu, Y. Sun, N. Kumar, L. Muechler, A. Sun, L. Jiao, S.-Y. Yang, D. Liu, A. Liang, Q. Xu, J. Kroder, V. Süß, H. Borrmann, C. Shekhar, Z. Wang, C. Xi, W. Wang, W. Schnelle, S. Wirth, Y. Chen *et al.*, *Nat. Phys.* **14**, 1125 (2018).
- [9] H. Chen, Q. Niu, and A. H. MacDonald, *Phys. Rev. Lett.* **112**, 017205 (2014).
- [10] Q. Wang, Y. Xu, R. Lou, Z. Liu, M. Li, Y. Huang, D. Shen, H. Weng, S. Wang, and H. Lei, *Nat. Commun.* **9**, 3681 (2018).
- [11] W.-H. Ko, P. A. Lee, and X.-G. Wen, *Phys. Rev. B* **79**, 214502 (2009).
- [12] B. R. Ortiz, S. M. L. Teicher, Y. Hu, J. L. Zuo, P. M. Sarte, E. C. Schueller, A. M. M. Abeykoon, M. J. Krogstad, S. Rosenkranz, R. Osborn, R. Seshadri, L. Balents, J. He, and S. D. Wilson, *Phys. Rev. Lett.* **125**, 247002 (2020).
- [13] B. R. Ortiz, L. C. Gomes, J. R. Morey, M. Winiarski, M. Bordelon, J. S. Mangum, I. W. H. Oswald, J. A. Rodriguez-Rivera, J. R. Neilson, S. D. Wilson, E. Ertekin, T. M. McQueen, and E. S. Toberer, *Phys. Rev. Materials* **3**, 094407 (2019).
- [14] Q. Yin, Z. Tu, C. Gong, Y. Fu, S. Yan, and H. Lei, *Chin. Phys. Lett.* **38**, 037403 (2021).
- [15] Y. Fu, N. Zhao, Z. Chen, Q. Yin, T. Tu, C. Gong, C. Xi, X. Zhu, Y. Sun, K. Liu, and H. Lei, *Phys. Rev. Lett.* **127**, 207002 (2021).
- [16] Y.-X. Jiang, J.-X. Yin, M. M. Denner, N. Shumiya, B. R. Ortiz, G. Xu, Z. Guguchia, J. He, M. S. Hossain, X. Liu, J. Ruff, L. Kautzsch, S. S. Zhang, G. Chang, I. Belopolski, Q. Zhang, T. A. Cochran, D. Multer, M. Litskevich, Z.-J. Cheng *et al.*, *Nat. Materials* **20**, 1353 (2021).

- [17] F. H. Yu, T. Wu, Z. Y. Wang, B. Lei, W. Z. Zhuo, J. J. Ying, and X. H. Chen, *Phys. Rev. B* **104**, L041103 (2021).
- [18] Z. Liang, X. Hou, F. Zhang, W. Ma, P. Wu, Z. Zhang, F. Yu, J. J. Ying, K. Jiang, L. Shan, Z. Wang, and X. H. Chen, *Phys. Rev. X* **11**, 031026 (2021).
- [19] Q. Wang, P. Kong, W. Shi, C. Pei, C. Wen, L. Gao, Y. Zhao, Q. Yin, Y. Wu, G. Li, H. Lei, J. Li, Y. Chen, and S. Yan, Y. Qi, *Adv. Mater. (Weinheim)* **33**, 2102813 (2021).
- [20] B. R. Ortiz, P. M. Sarte, E. M. Kenney, M. J. Graf, S. M. L. Teicher, R. Seshadri, and S. D. Wilson, *Phys. Rev. Materials* **5**, 034801 (2021).
- [21] S.-Y. Yang, Y. Wang, B. R. Ortiz, D. Liu, J. Gayles, E. Derunova, R. Gonzalez-Hernandez, L. Šmejkal, Y. Chen, S. S. P. Parkin, S. D. Wilson, E. S. Toberer, T. McQueen, and M. N. Ali, *Sci. Adv.* **6**, eabb6003 (2020).
- [22] B. Sipos, A. F. Kusmartseva, A. Akrap, H. Berger, L. Forró, and E. Tutiš, *Nat. Mater.* **7**, 960 (2008).
- [23] Q. Dong, Q. Li, S. Li, X. Shi, S. Niu, S. Liu, R. Liu, B. Liu, X. Luo, J. Si, W. Lu, N. Hao, Y. Sun, and B. Liu, *npj Quantum Mater.* **6**, 20 (2021).
- [24] X.-C. Pan, X. Chen, H. Liu, Y. Feng, Z. Wei, Y. Zhou, Z. Chi, L. Pi, F. Yen, F. Song, X. Wan, Z. Yang, B. Wang, G. Wang, and Y. Zhang, *Nat. Commun.* **6**, 7805 (2015).
- [25] Y. Qi, P. G. Naumov, M. N. Ali, C. R. Rajamathi, W. Schnelle, O. Barkalov, M. Hanfland, S.-C. Wu, C. Shekhar, Y. Sun, V. Süß, M. Schmidt, U. Schwarz, E. Pippel, P. Werner, R. Hillebrand, T. Förster, E. Kampert, S. Parkin, R. J. Cava *et al.*, *Nat. Commun.* **7**, 11038 (2016).
- [26] F. H. Yu, D. H. Ma, W. Z. Zhuo, S. Q. Liu, X. K. Wen, B. Lei, J. J. Ying, and X. H. Chen, *Nat. Commun.* **12**, 3645 (2021).
- [27] K. Y. Chen, N. N. Wang, Q. W. Yin, Y. H. Gu, K. Jiang, Z. J. Tu, C. S. Gong, Y. Uwatoko, J. P. Sun, H. C. Lei, J. P. Hu, and J. G. Cheng, *Phys. Rev. Lett.* **126**, 247001 (2021).
- [28] F. Du, S. Luo, B. R. Ortiz, Y. Chen, W. Duan, D. Zhang, X. Lu, S. D. Wilson, Y. Song, and H. Yuan, *Phys. Rev. B* **103**, L220504 (2021).
- [29] C. C. Zhu, X. F. Fang, W. Xia, Q. W. Yin, L. S. Wang, C. C. Zhao, D. Z. Dai, C. P. Tu, B. Q. Song, Z. C. Tao, Z. J. Tu, C. S. Gong, H. C. Lei, Y. F. Guo, and S. Y. Li, *arXiv:2104.14487*.
- [30] N. N. Wang, K. Y. Chen, Q. W. Yin, Y. N. N. Ma, B. Y. Pan, X. Yang, X. Y. Ji, S. L. Wu, P. F. Shan, S. X. Xu, Z. J. Tu, C. S. Gong, G. T. Liu, G. Li, Y. Uwatoko, X. L. Dong, H. C. Lei, J. P. Sun, and J. G. Cheng, *Phys. Rev. Res.* **3**, 043018 (2021).
- [31] Z. Zhang, Z. Chen, Y. Zhou, Y. Yuan, S. Wang, J. Wang, H. Yang, C. An, L. Zhang, X. Zhu, Y. Zhou, X. Chen, J. Zhou, and Z. Yang, *Phys. Rev. B* **103**, 224513 (2021).
- [32] X. Chen, X. Zhan, X. Wang, J. Deng, X.-B. Liu, X. Chen, J.-G. Guo, and X. Chen, *Chin. Phys. Lett.* **38**, 057402 (2021).
- [33] C. C. Zhao, L. S. Wang, W. Xia, Q. W. Yin, J. M. Ni, Y. Y. Huang, C. P. Tu, Z. C. Tao, Z. J. Tu, C. S. Gong, H. C. Lei, Y. F. Guo, X. F. Yang, and S. Y. Li, *arXiv:2102.08356*.
- [34] P. Giannozzi, S. Baroni, N. Bonini, M. Calandra, R. Car, C. Cavazzoni, D. Ceresoli, G. L. Chiarotti, M. Cococcioni, I. Dabo, A. Dal Corso, S. de Gironcoli, S. Fabris, G. Fratesi, R. Gebauer, U. Gerstmann, C. Gougoussis, A. Kokalj, M. Lazzeri, L. Martin-Samos *et al.*, *J. Phys.: Condens. Matter* **21**, 395502 (2009).
- [35] D. Vanderbilt, *Phys. Rev. B* **41**, 7892 (1990).
- [36] J. P. Perdew, K. Burke, and M. Ernzerhof, *Phys. Rev. Lett.* **77**, 3865 (1996).
- [37] S. Grimme, J. Antony, S. Ehrlich, and H. Krieg, *J. Chem. Phys.* **132**, 154104 (2010).
- [38] S. Baroni, S. de Gironcoli, A. Dal Corso, and P. Giannozzi, *Rev. Mod. Phys.* **73**, 515 (2001).
- [39] M. J. Verstraete, M. Torrent, F. Jollet, G. Zérah, and X. Gonze, *Phys. Rev. B* **78**, 045119 (2008).
- [40] V. Chis, I. Y. Sklyadneva, K. A. Kokh, V. A. Volodin, O. E. Tereshchenko, and E. V. Chulkov, *Phys. Rev. B* **86**, 174304 (2012).
- [41] B.-T. Wang, P. Zhang, R. Lizarraga, I. Di Marco, and O. Eriksson, *Phys. Rev. B* **88**, 104107 (2013).
- [42] M. P. L. Sancho, J. M. L. Sancho, and J. Rubio, *J. Phys. F: Met. Phys.* **15**, 851 (1985).
- [43] Q. Wu, S. Zhang, H.-F. Song, M. Troyer, and A. A. Soluyanov, *Comput. Phys. Commun.* **224**, 405 (2018).
- [44] I. Souza, N. Marzari, and D. Vanderbilt, *Phys. Rev. B* **65**, 035109 (2001).
- [45] N. Marzari, A. A. Mostofi, J. R. Yates, I. Souza, and D. Vanderbilt, *Rev. Mod. Phys.* **84**, 1419 (2012).
- [46] H. Tan, Y. Liu, Z. Wang, and B. Yan, *Phys. Rev. Lett.* **127**, 046401 (2021).
- [47] Z. Liu, N. Zhao, Q. Yin, C. Gong, Z. Tu, M. Li, W. Song, Z. Liu, D. Shen, Y. Huang, K. Liu, H. Lei, and S. Wang, *Phys. Rev. X* **11**, 041010 (2021).
- [48] H. Zhao, H. Li, B. R. Ortiz, S. M. L. Teicher, T. Park, M. Ye, Z. Wang, L. Balents, S. D. Wilson, and I. Zeljko, *Nature (London)* **599**, 216 (2021).
- [49] H. Chen, H. Yang, B. Hu, Z. Zhao, J. Yuan, Y. Xing, G. Qian, Z. Huang, G. Li, Y. Ye, S. Ma, S. Ni, H. Zhang, Q. Yin, C. Gong, Z. Tu, H. Lei, H. Tan, S. Zhou, C. Shen *et al.*, *Nature (London)* **599**, 222 (2021).
- [50] S. Ni, S. Ma, Y. Zhang, J. Yuan, H. Yang, Z. Lu, N. Wang, J. Sun, Z. Zhao, D. Li, S. Liu, H. Zhang, H. Chen, K. Jin, J. Cheng, L. Yu, F. Zhou, X. Dong, J. Hu, H.-J. Gao *et al.*, *Chin. Phys. Lett.* **38**, 057403 (2021).
- [51] X. Zhou, Y. Li, X. Fan, J. Hao, Y. Dai, Z. Wang, Y. Yao, and H.-H. Wen, *Phys. Rev. B* **104**, L041101 (2021).
- [52] M. Kang, S. Fang, J.-K. Kim, B. R. Ortiz, S. H. Ryu, J. Kim, J. Yoo, G. Sangiovanni, D. D. Sante, B.-G. Park, C. Jozwiak, A. Bostwick, E. Rotenberg, E. Kaxiras, S. D. Wilson, J.-H. Park, and R. Comin, *Nat. Phys.* (2022), doi:10.1038/s41567-021-01451-5.
- [53] See Supplemental Material at <http://link.aps.org/supplemental/10.1103/PhysRevB.105.024517> for parity of wave function, band structure with SOC and electron susceptibility under ambient pressure, phonon dispersions of CsV₃Sb₅ under 50 GPa, atomic-orbital-resolved band structure, density of states, and total DOS for 2, 15, and 45 GPa.
- [54] H. Li, T. T. Zhang, T. Yilmaz, Y. Y. Pai, C. E. Marvinney, A. Said, Q. W. Yin, C. S. Gong, Z. J. Tu, E. Vescovo, C. S. Nelson, R. G. Moore, S. Murakami, H. C. Lei, H. N. Lee, B. J. Lawrie, and H. Miao, *Phys. Rev. X* **11**, 031050 (2021).
- [55] K. Nakayama, Y. Li, T. Kato, M. Liu, Z. Wang, T. Takahashi, Y. Yao, and T. Sato, *Phys. Rev. B* **104**, L161112 (2021).
- [56] H. W. Myron and A. J. Freeman, *Phys. Rev. B* **11**, 2735 (1975).
- [57] C. Battaglia, H. Cercellier, F. Clerc, L. Despont, M. G. Garnier, C. Koitzsch, P. Aebi, H. Berger, L. Forró, and C. Ambrosch-Draxl, *Phys. Rev. B* **72**, 195114 (2005).
- [58] Y. Liu, D. F. Shao, L. J. Li, W. J. Lu, X. D. Zhu, P. Tong, R. C. Xiao, L. S. Ling, C. Y. Xi, L. Pi, H. F. Tian, H. X. Yang, J. Q. Li,

- W. H. Song, X. B. Zhu, and Y. P. Sun, *Phys. Rev. B* **94**, 045131 (2016).
- [59] M. D. Johannes and I. I. Mazin, *Phys. Rev. B* **77**, 165135 (2008).
- [60] A. Y. Liu, *Phys. Rev. B* **79**, 220515(R) (2009).
- [61] C. Chen, B. Singh, H. Lin, and V. M. Pereira, *Phys. Rev. Lett.* **121**, 226602 (2018).
- [62] J. van Wezel, P. Nahai-Williamson, and S. S. Saxena, *Phys. Rev. B* **81**, 165109 (2010).
- [63] C. Wang, S. Liu, H. Jeon, and J.-H. Cho, [arXiv:2109.01921](https://arxiv.org/abs/2109.01921).
- [64] J. G. Si, W. J. Lu, H. Y. Wu, H. Y. Lv, X. Liang, Q. J. Li, and Y. P. Sun, *Phys. Rev. B* **101**, 235405 (2020).
- [65] A. W. Tsen, R. Hovden, D. Wang, Y. D. Kim, J. Okamoto, K. A. Spoth, Y. Liu, W. Lu, Y. Sun, J. C. Hone, L. F. Kourkoutis, P. Kim, and A. N. Pasupathy, *Proc. Natl. Acad. Sci. USA* **112**, 15054 (2015).
- [66] B.-T. Wang, P. F. Liu, J.-J. Zheng, W. Yin, and F. Wang, *Phys. Rev. B* **98**, 014514 (2018).
- [67] X. Xi, L. Zhao, Z. Wang, H. Berger, L. Forró, J. Shan, and K. F. Mak, *Nat. Nanotechnol.* **10**, 765 (2015).
- [68] M. M. Ugeda, A. J. Bradley, Y. Zhang, S. Onishi, Y. Chen, W. Ruan, C. Ojeda-Aristizabal, H. Ryu, M. T. Edmonds, H.-Z. Tsai, A. Riss, S.-K. Mo, D. Lee, A. Zettl, Z. Hussain, Z.-X. Shen, and M. F. Crommie, *Nat. Phys.* **12**, 92 (2016).
- [69] R. C. Dynes, *Soild State Commun.* **10**, 615 (1972).
- [70] P. B. Allen and R. C. Dynes, *Phys. Rev. B* **12**, 905 (1975).
- [71] P. B. Allen and B. Mitrović, *Solid State Phys.* **37**, 1 (1983).
- [72] J. Kortus, I. I. Mazin, K. D. Belashchenko, V. P. Antropov, and L. L. Boyer, *Phys. Rev. Lett.* **86**, 4656 (2001).
- [73] B.-T. Wang, P. Zhang, H.-Y. Liu, W.-D. Li, and P. Zhang, *J. Appl. Phys. (Melville, NY)* **109**, 063514 (2011).
- [74] R. C. Xiao, W. J. Lu, D. F. Shao, J. Y. Li, M. J. Wei, H. Y. Lv, P. Tong, X. B. Zhu, and Y. P. Sun, *J. Mater. Chem. C* **5**, 4167 (2017).
- [75] J.-F. Zhang, K. Liu, and Z.-Y. Lu, *Phys. Rev. B* **104**, 195130 (2021).
- [76] H.-S. Xu, Y.-J. Yan, R. Yin, W. Xia, S. Fang, Z. Chen, Y. Li, W. Yang, Y. Guo, and D.-L. Feng, *Phys. Rev. Lett.* **127**, 187004 (2021).
- [77] M. L. Kiesel, C. Platt, W. Hanke, D. A. Abanin, and R. Thomale, *Phys. Rev. B* **86**, 020507(R) (2012).
- [78] E. R. Margine and F. Giustino, *Phys. Rev. B* **90**, 014518 (2014).
- [79] R. Nandkishore, L. S. Levitov, and A. V. Chubukov, *Nat. Phys.* **8**, 158 (2012).
- [80] K. Kim, S. Kim, J. S. Kim, H. Kim, J. H. Park, and B. I. Min, *Phys. Rev. B* **97**, 165102 (2018).